



Deriving atmospheric turbulence intensity from profiling pulsed lidar measurements

Maxime Thiébaud¹, Marie Cathelain¹, Salma Yahiaoui², and Ahmed Esmail³

¹France Énergies Marines, Technopôle Brest-Iroise, 525 Avenue Alexis de Rochon, 29280 Plouzané, France

²Vaisala France SAS, 6A, rue René Razel, Tech Park, CS 70001, 91400 Saclay Cedex, France

³GL Garrad Hassan Deutschland GmbH, Loads & Power Performance & Wind Resource (E-NX-RL), Sommerdeich 14b, 25709 Kaiser-Wilhelm-Koog, Germany

Correspondence: Maxime Thiébaud (maxime.thiebaud@france-energies-marines.org)

Abstract. A new method is proposed to provide estimates of the turbulence intensity (TI) from measurements of pulsed lidars (light detection and ranging) employing the Doppler beam swinging technique. This method relies on combining the variances of the line-of-sight (LOS) velocities collected by the five independent beams of the lidars and, as such, is referred to as the variance method. The variance method comes with an explicit removal of the Doppler noise (inherent to the instrument) to the variance of the LOS velocities. Turbulence metrics derived from the variance method are compared to that derived from a standard method, commonly used in the wind energy industry. Reference turbulence measurements are provided by a sonic anemometer mounted on a meteorological mast, installed nearby the lidars. Two configurations of the WindCube v2.1 lidars are proposed: the commercial configuration and a prototype configuration, sampling 4 times faster, thus allowing to capture the turbulent energy of smaller eddies. The standard method applied on wind measurements collected by both configurations shows mean errors in TI estimates of more than 50%. The application of the variance method on measurements collected by the commercial and prototype configuration drops the mean error to 16.7% and 13.2% respectively.

1 Introduction

A comprehensive assessment of the inflow conditions is highly important for an optimal planning and design of wind energy projects. More specifically, the measurement of the ambient turbulence is critical to gain confidence in the representativeness of the aerodynamic loading on wind turbine structures and the modeling of future wind farms effects, i.e., impacts on the atmospheric flow by the single wind turbines, within wind farms, and large clusters (Rohrig et al., 2019; Veers et al., 2019). In particular, the knowledge of the turbulence intensity, TI, is essential since TI is directly involved in modeling applications of wake effects within wind farms which can significantly decrease the power production and increase the cost of electricity (Howland et al., 2019). Turbulence is also known to affect the lifetime of certain turbine components (e.g., blades, rotor, tower) and thus, are highly relevant for questions of potential lifetime extensions (Kelley et al., 2005, 2006). Moreover, wind turbine performance is impacted by turbulence levels and wind shear driven by atmospheric stability (Wharton and Lundquist, 2012; Clifton and Wagner, 2014).



In the wind power industry, the characterization of ambient turbulence through measurements of meteorological mast anemometry is the traditional method. Either cup or sonic anemometers are mounted on slender booms at several altitudes
25 over a certain period of time. However, wind turbines have experienced a continuous growth in size in the past decades and the upper tip of onshore wind turbines blade can now easily reach heights up to 200 m above the ground. This increases the needs for wind and turbulence measurements at higher altitudes. Collecting measurements at such height with meteorological masts is non longer a viable solution since installing and operating such massive infrastructures is cost-prohibitive.

In response, remote sensing devices such as profiling lidars (light detection and ranging) have recently emerged as alter-
30 natives to meteorological masts. Measurement methods used by lidars are fundamentally different than those used by cup or sonic anemometers. Anemometers provide an estimate of the wind speed across a volume a few cubic centimeters whereas lidars provide an average across a probe volume of up to several dozen cubic meters. This system can be categorized according to their emission waveform, i.e., pulsed or continuous, and measuring technique, i.e., Doppler beam swinging (DBS) (Strauch et al., 1984) or velocity-azimuth display (VAD) (Browning and Wexler, 1968). Lidar systems offer the potential for reduced
35 costs compared to meteorological masts and the ability to measure at the same or even greater heights above the ground.

While profiling lidars have proven to be accurate tools for measuring mean wind speed and direction (Smith et al., 2006; Emeis et al., 2007; Sjöholm et al., 2008; Wagner et al., 2011; Gottschall et al., 2012; Kim et al., 2016) they are still not accepted for turbulence measurements which is an active area of research (Sathe et al., 2015; Newman et al., 2016). This lack of acceptance is mainly due to, (1), large measurement volumes leading to spatial averaging of turbulence along the line-
40 of-sight (LOS), (2), cross-contamination by different turbulent structures of the wind field, (3), low sampling rate, and , (4), instrument noise. The present paper will address the second, third, and fourth limitations.

The spectral signature of the cross-contamination effect has been clearly identified in turbulent kinetic energy (TKE) spectra, i.e., velocity variance as a function of frequency, by an almost complete attenuation of the turbulence signal in the inertial sub-range (Canadillas et al., 2010; Sathe and Mann, 2012; Kelberlau and Mann, 2020) preceded by a hump of energy generated by
45 the beam interference phenomenon. This phenomenon induces additional variance to the signal which causes an overestimation of TI.

In this paper, the low sampling rate is tackled by proposing, for the first time, the deployment of a WindCube v2.1 lidar with a sampling rate four times higher than the commercial technology. This faster sampling rate configuration is expected to capture smaller eddies and their associated turbulent energy thus allowing for more accurate estimation of turbulence. Synchronous
50 measurements of the lidar operating with a faster sampling rate configuration, alongside with measurements of a commercial lidar is proposed to assess the benefit of the new configuration.

Finally, the instrument noise correction is addressed. Among the four limitations of the lidars, instrument noise correction is less explored and, as far as we know, not documented in the literature. This specific topic could benefit from recent works carried out in the field of ocean engineering. In ocean science, acoustic Doppler current profilers (ADCP) are often the standard
55 instrument for measuring flow speed and turbulence at different depth levels, throughout the water column. Recently, five-beam ADCP has been commercialized (Guerra and Thomson, 2017). The configuration of such sensors is similar to the WindCube v2.1 lidars configuration with four-diverging beams and a fifth beam pointing vertically upward. Both five-beam ADCPs and

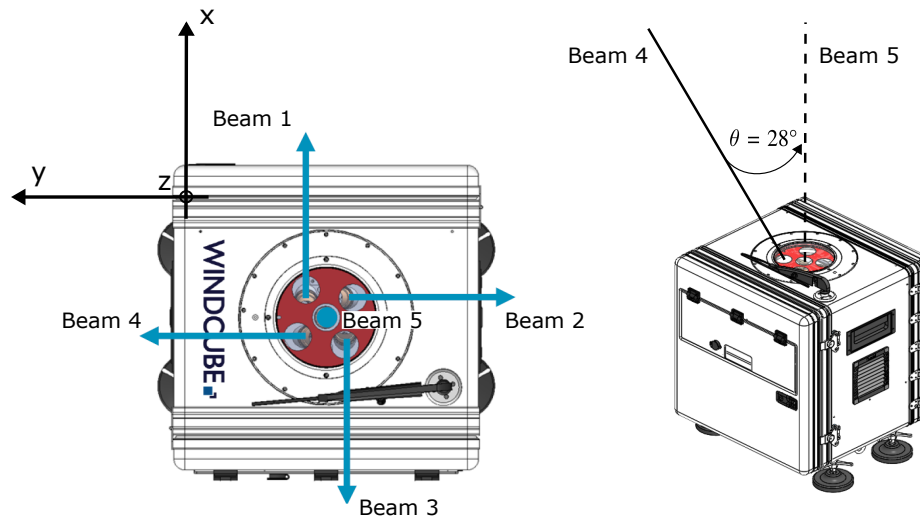


Figure 1. Left: top view of a WindCube v2.1 lidar with positions of its five beams. The x component is oriented from beam 3 towards beam 1, the y component points from beam 4 towards beam 2, and the vertical z component points downwards along Beam 5. Right : tridimensional view with the angle of beam inclination $\theta = 28^\circ$.

WindCube v2.1 lidars employ the Doppler effect through backscattered signal of emitted pulses in order to measure the flow velocity at different heights above instrument. However, measurements based on Doppler effect are affected by the Doppler noise, inherent to the instrument, which produces significant overestimation in the calculation of turbulence metrics. In the field of ocean engineering, this effect has been clearly identified and methods have been developed to correct turbulence measurements from the Doppler noise-induced variance resulting in a substantial improvement of the turbulence estimation (Thomson et al., 2010, 2012; Richard et al., 2013; Durgesh et al., 2014; Thiébaud et al., 2020a, b). Considering similarities in the measurements principles between ADCPs and pulsed lidars, it is expected that Doppler noise also strongly affects turbulence estimates derived from measurements of pulsed lidars.

In this paper, a method used for correcting Doppler noise of oceanographic measurements is transposed to improve atmospheric measurements. The method is tested on simultaneous measurements collected by two pulsed lidars employing the DBS technique with two different sampling rates. Reference turbulence measurements are provided by a sonic anemometer mounted on a meteorological mast, installed nearby the lidars. The focus is on the altitude matching the position of the sonic anemometer. Variances of the LOS velocities provided by the lidars are corrected from the Doppler noise-induced variance and combined through trigonometric expressions proposed by Dewey and Stringer (2007), originally dedicated to ocean engineering applications. This method relies on combining the variances of velocity measurements collected by five independent beams and, as such, is referred to as the variance method. This method attenuates the cross-contamination effect and allows for a considerable improvement of turbulence metrics.



75 2 Data collection and methods

2.1 WindCube v2.1 - commercial and prototype configuration

The measurement of wind speed and direction derived from a commercial WindCube v2.1 lidar is based on the pulsed Doppler heterodyne laser principle. The lidar sends tenths of thousands 175 ns long laser pulses in the atmosphere. Light pulses are backscattered by aerosols and, from those received, Doppler shift is analyzed before the next laser pulse is emitted. This avoids
80 confusing time delays and distances. Therefore, probe distance, or height, only depends on the time it takes for a pulse to be received after it has been emitted.

The WindCube v2.1 enables wind profile measurement from 40 meters to 300 meters through up to 20 independently configurable measurement heights. The WindCube v2.1 technology ensures a 20-m long constant probe volume of atmosphere which leads to constant accuracy at all heights. Four beams are sent successively in four cardinal directions along a 28° scanning
85 cone angle, followed by a fifth, pointing vertically upward and providing a direct estimate of the vertical velocity. The LOS velocities (i.e. radial velocities) are measured simultaneously at each configured height before switching to another beam. The sampling rate of the LOS velocities of the commercial WindCube v2.1, hereinafter referred to as “commercial configuration”, is $f_c = 0.25$ Hz. The sampling rate, f_p , of the LOS velocities of the new configuration, hereinafter referred to as “prototype configuration”, is four times faster, i.e., $f_p = 1$ Hz.

90 2.2 Coordinate system and preliminaries

The LOS velocities are combined to calculate the horizontal components (V_x and V_y) of the wind speed in the instrument coordinate system which is a left-handed coordinate system defined by the beam directions. The x component is oriented from beam 3 towards beam 1, the y component points from beam 4 towards beam 2, and the vertical z component points downwards along Beam 5 (Fig. 1). Defining the wind field in the direction of beam i as b_i , with positive velocity being towards
95 the instrument, the coordinate transformation from beam coordinates to instrument coordinates is given by Eq. 1 and 2:

$$V_x = \frac{b_1 - b_3}{2 \sin\theta} \quad (1)$$

$$V_y = \frac{b_2 - b_4}{2 \sin\theta} \quad (2)$$

where $\theta = 28^\circ$ is the angle of divergence of each beam position from the vertical, i.e., the beam inclination angle.

100 2.3 Turbulence intensity

The turbulence intensity, TI, is the most common metric used in the wind energy industry as well as other engineering fields in order to quantify turbulence. TI is referred to as the turbulence level and represents the intensity of velocity fluctuations. TI



is an input specification for synthetic turbulence generators such as TurbSim (Jonkman and Kilcher, 2012). These simulations require inflow turbulence conditions for calculations of dynamic forces acting on wind turbines.

105 In this work, TI is estimated from two methods. The first method, hereinafter referred to as the "standard method", uses the velocity in instrument coordinates. This method leads to the variance contamination errors discussed in the literature (Sathe and Mann, 2012; Kelberlau and Mann, 2020) and substantial overestimation of TI. The standard method is used as comparison to the novel method presented in this paper. This method, hereinafter referred to as the "variance method", uses the variance of the LOS velocities with an explicit removal of the Doppler noise to estimate TI. The subscripts "s" and "v" are used to identify
110 the standard and variance method respectively.

2.3.1 Standard method

The turbulence intensity, TI_s , computed from the standard method is given by:

$$TI_s = \frac{\sqrt{(\overline{V_x'^2} + \overline{V_y'^2})/2}}{U} \quad (3)$$

115 where the prime denotes a fluctuation from the mean component, and U is the 10-min averaged horizontal wind speed. The overbar is used to represent a temporal average.

2.3.2 Variance method

The variance of the LOS velocity, \hat{b}'_i , recorded by a WindCube v2.1 along the i -th beam is the sum of the « true » turbulent velocity, b'_i , and an error, n_i , associated with Doppler noise such that:

$$\hat{b}'_i = b'_i + n_i \quad (4)$$

120 n_i is regularly approximated as Gaussian white noise (Thomson et al., 2012; Richard et al., 2013; Durgesh et al., 2014; Guerra and Thomson, 2017; McMillan and Hay, 2017; Thiébaud et al., 2020a, b) with a constant spectral density, N_i , and a variance, n_i^2 , such that:

$$n_i^2 = N_i \times f_N \quad (5)$$

where f_N is the Nyquist frequency.

125 The variance method applied on the five beams of the WindCube v2.1 ensures the estimation of five (out of six) components of the Reynolds stress tensor \mathbf{R} (Eq. 6). Only the horizontal shear, $\overline{u'v'}$, remains unknown.

$$\mathbf{R} = \begin{pmatrix} \overline{u'^2} & \overline{u'v'} & \overline{u'w'} \\ \overline{u'v'} & \overline{v'^2} & \overline{v'w'} \\ \overline{u'w'} & \overline{v'w'} & \overline{w'^2} \end{pmatrix} \quad (6)$$

The five Reynolds stresses are calculated following the Dewey and Stringer's formulations (Dewey and Stringer, 2007). In the present paper, the horizontal TI derived from the variance method involves two components of the Reynolds stress tensor, $\overline{u'^2}$



130 and $\overline{v'^2}$ such as:

$$TI_v = \frac{\sqrt{(u'^2 + v'^2)}/2}{U} \quad (7)$$

$\overline{u'^2}$ and $\overline{v'^2}$ are given by Eq. 8 and 9 respectively. The vertical stress $\overline{w'^2}$ (Eq. 10) is also addressed for a specific analysis dedicated to the comparison of $\overline{w'^2}$ with the vertical stress, $\overline{b'_5{}^2}$, directly measured by Beam 5. In Eq. 8, 9 and 10, $\overline{b'_i{}^2} = \widehat{b'_i{}^2} - n_i^2$ and ϕ_1 and ϕ_2 correspond to Dewey and Stringer's pitch and roll. For the WindCube v2.1 coordinate system, ϕ_1 corresponds to roll and ϕ_2 corresponds to negative pitch (Guerra and Thomson, 2017).

$$\overline{u'^2} = \frac{-1}{4 \sin^6 \theta \cos^2 \theta} \left(-2 \sin^4 \theta \cos^2 \theta (\overline{b'_3{}^2} + \overline{b'_1{}^2} - 2 \cos^2 \theta \overline{b'_5{}^2}) + 2 \sin^5 \theta \cos \theta \phi_2 (\overline{b'_3{}^2} - \overline{b'_1{}^2}) \right) \quad (8)$$

$$\overline{v'^2} = \frac{-1}{4 \sin^6 \theta \cos^2 \theta} \left(-2 \sin^4 \theta \cos^2 \theta (\overline{b'_2{}^2} + \overline{b'_4{}^2} - 2 \cos^2 \theta \overline{b'_5{}^2}) - 2 \sin^4 \theta \cos^2 \theta \phi_2 (\overline{b'_3{}^2} - \overline{b'_1{}^2}) + 2 \sin^3 \theta \cos^3 \theta \phi_2 (\overline{b'_3{}^2} - \overline{b'_1{}^2}) - 2 \sin^5 \theta \cos \theta \phi_1 (\overline{b'_2{}^2} - \overline{b'_4{}^2}) \right) \quad (9)$$

$$\overline{w'^2} = \frac{-1}{4 \sin^6 \theta \cos^2 \theta} \left(-2 \sin^5 \theta \cos \theta \phi_2 (\overline{b'_3{}^2} - \overline{b'_1{}^2}) + 2 \sin^5 \theta \cos \theta \phi_1 (\overline{b'_2{}^2} - \overline{b'_4{}^2}) - 4 \sin^6 \theta \cos^2 \theta \overline{b'_5{}^2} \right) \quad (10)$$

Note that $\overline{V_x'^2}$, involves in the calculation of TI_s , and $\overline{u'^2}$, involves in the calculation of TI_v , are the variances of the wind component associated with the same x -direction (Fig. 1) and should be equal, in theory. They are however different since they are both estimated from two distinct methods. A different notation has been used on purpose to avoid confusion. The same remarks can be made for $\overline{V_y'^2}$ and $\overline{v'^2}$.

2.4 Field measurements

2.4.1 Meteorological mast

145 The field measurements campaign was carried out by DNV-GL at the lidar validation measurement test site in Janneby, Germany (Fig. 2). Due to its flat terrain, the site has good atmospheric conditions for the purposes of verification trials of lidar systems. The site has a good exposure to largely undisturbed wind condition, i.e., undisturbed winds from almost all sectors. The elevation of the site is a few meters above mean sea level. The surface roughness is low due to a mainly agricultural land use (Fig. 2b). Two wind turbines (WT N100 and WT N117 in Fig. 2b) are installed in the vicinity of the meteorological mast.

150 The closest wind turbine is located 210 m from the mast.

The meteorological mast is a 3-fold guyed 100 m lattice tower with a constant face width of 0.4 m over its entire extension. Six MEASNET calibrated cup anemometers of type Thies First Class Advanced (No. 4.3351) and a sonic anemometer from Thies Clima are mounted on the mast. The mounting arrangements are consistent with the currently valid IEC and IEA recommendations for the use of cup anemometry at meteorological masts. As can be seen in Fig. 2c, two cup anemometers are

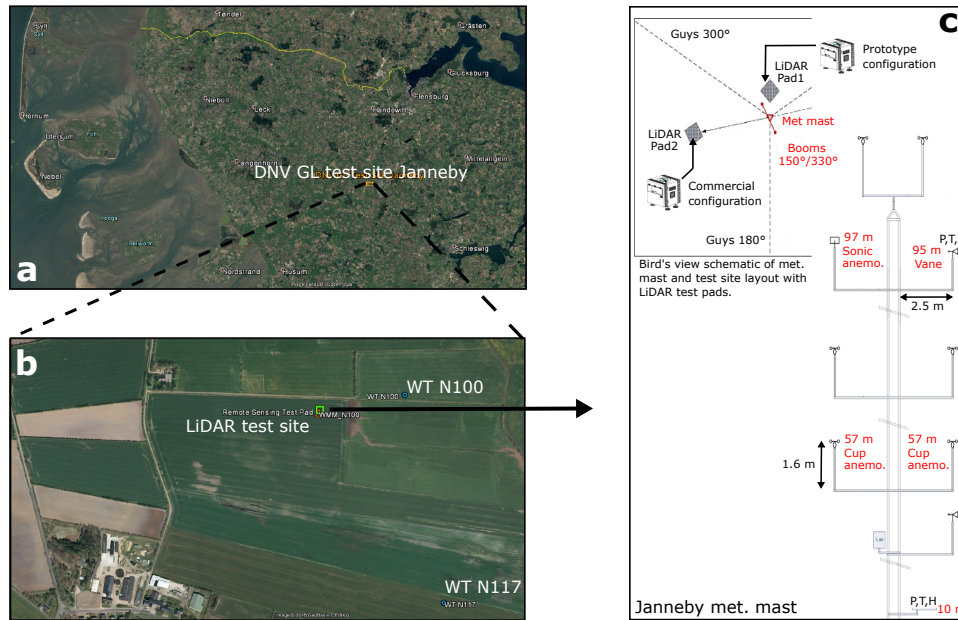


Figure 2. Map (a) and inlet map (b) of test site location at Janneby, Germany. The meteorological mast configuration is shown in (c). Only the instrumentation used in this study is shown.

155 mounted on booms pointing towards 150° and 330° at 57 m, 76 m and 100 m above ground. The sonic anemometer is pointing
toward 150° and mounted at 97 m above ground. This altitude corresponds to the average hub height of modern land-based
wind turbines. The cup and sonic anemometers were set to record the wind speed and direction at sampling rate of 1 Hz and 4
Hz respectively. In addition to wind measurements, 10-minute averaged temperature, humidity and pressure were measured at
10 m and 95 m above ground.

160 2.4.2 Data collection

The field measurements campaign was conducted during two periods, from 12 to 25 November 2021 and from 07 December
2021 to 10 January 2022. Both measurement periods were combined to form a 47-day dataset. For the purpose of this paper,
the focus is on 97-m altitude, which matches the position of the sonic anemometer. TI derived from the sonic anemometer are
the reference for the comparison with TI derived from the measurements of the commercial and prototype WindCube lidars.

165 The sonic anemometer was set to record continuously the horizontal wind speed and wind direction at a sampling rate of 4
Hz. Both horizontal wind speed and direction were used to derive the two horizontal wind velocity components thus allowing
for the calculation of the reference TI. The comparison of TI derived from the commercial and prototype configuration imposed
to resample the sonic-derived wind dataset to a rate that matches the sampling rate of the LOS velocities measured by both
configurations. This allows to ensure that similar turbulence time scales are captured when calculating and comparing the



170 turbulence metrics. Thus, measurements of the sonic anemometer were resampled at $f_c = 0.25$ Hz and $f_p = 1$ Hz for the comparison of the reference TI against TI derived from the commercial and prototype configuration respectively.

The 47-day dataset was divided into 6762 subsets of 10-min data records giving subsets containing 150 and 600 measurement points for wind data acquisition at a sampling rate of 0.25 Hz and 1 Hz respectively. The 10-min duration is long enough to retain the longest time scales of coherent turbulent structures in the turbulent fluctuations. This duration is also appropriate
175 to support the hypothesis that the turbulent processes cannot be regarded as quasi-stationary (i.e., stable mean and variance), which is essential for calculating turbulence metrics and turbulence velocity spectra. Note that, instead of 10-min, previous works divided their dataset into 30-min of data records (Sathe et al., 2015; Newman et al., 2016) in order to reduce the noise on variance estimates.

2.5 Data selection

180 The presence of two wind turbines in the vicinity of the meteorological mast required a data filtering to ensure that the wind data are not disturbed by the turbines wake. Considering North as reference, 10-min subsets associated with a wind direction comprised in the intervals $[60^\circ; 100^\circ]$ and $[130^\circ; 170^\circ]$ were rejected, as recommended by DNV-GL. As a result, 18.9% of the 6762 10-min subsets was excluded from the analysis. The wind direction for the sector filtering was given by the wind vane mounted on the meteorological mast at 95 m height above ground.

185 A second filtering was performed on the 5484 remaining subsets. This step consisted in rejecting the 10-min subsets associated with a data availability lower than 75%. This step was performed on the velocity time series derived from the sonic anemometer and that derived from each beam of the commercial and prototype lidars. A percentage ranging from 0.6 to 1.7%, varying according to the beams of the commercial lidar was rejected. For the prototype lidar, this percentage was found to be 2 to 3 times higher depending on the beam. Since the normal stresses are calculated using a combination of the LOS velocities,
190 the exclusion of a 10-min subset associated with one single beam will not make possible the calculation of the normal stresses and thus, the associated TI. The second filtering resulted in the rejection of 16.4% of subsets remaining from the first filtering. After both filtering steps, 4336 10-min subsets were considered as valid for the turbulence analysis.

2.6 Data classification

The 4336 10-min subsets were classified according to the atmospheric stability and split into two groups: unstable and stable
195 conditions. The classification was done through the calculation of the Richardson number, R_i , defined as:

$$R_i = \frac{g(dT/dz + \Gamma_d)}{T(dU/dz)^2} \quad (11)$$

where g is the gravitational acceleration, T , the absolute mean temperature, $\Gamma_d = 0.0098 \text{ K.m}^{-1}$, the dry adiabatic lapse rate and (dT/dz) and (dU/dz) , the vertical gradients of the absolute temperature and horizontal wind speed respectively. Temperature was measured from a sensor mounted on the meteorological mast at 95 m and 10 m height above ground, given $T_{95\text{m}}$ and
200 $T_{10\text{m}}$. Horizontal wind speed was measured from the sonic anemometer supplemented by cup anemometers mounted on the



mast at 57 m height above ground, given U_{97m} and U_{57m} . Thus, Eq. 11 becomes:

$$R_i = \frac{g[(T_{95m} - T_{10m})/\Delta z_T + \Gamma_d]\Delta z_U^2}{T_{10m}(U_{97m} - U_{57m})^2} \quad (12)$$

where $\Delta z_T = 85$ m and $\Delta z_U = 40$ m correspond to the difference in measurements altitudes for T and U respectively. A convective unstable wind flow is associated with $R_i < 0$ while stable wind flow is associated with $R_i > 0$. Among the 4336
205 10-min subsets, 10.6% were recorded during unstable conditions whereas 89.4% were recorded during stable conditions.

3 Results

3.1 Turbulent kinetic energy spectra

Turbulent kinetic energy spectra (hereafter referred to as ‘spectra’) allow the determination of the distribution of turbulent energy as a function of frequency, i.e., spectra quantify the amount of energy in the flow at a range of time scales. In theory,
210 spectra are supposed to exhibit an inertial frequency subrange where the slope follows the classic $f^{-5/3}$ slope associated with the energy cascade (Frish, 1995; Pope, 2000). In the inertial subrange, the assumption of local isotropy holds over a range of length scales associated with the velocity fluctuations and a range of length scales associated with eddy size. Note that the term “local isotropy” refers only to the small-scales turbulent motions. The inertial subrange does not take into account the very large scale (the integral length scale), where the energy is injected into the system by the external forces, nor does it include
215 the very small scale (the Kolmogorov microscale, η), where the energy is dissipated into heat by viscosity.

Spectra of the LOS velocities associated with each beam of the commercial and prototype lidars were investigated to determine the constant spectral densities N_i , signature of the Doppler noise and thus, calculate the Doppler noise-induced variance n_i^2 . In Fig. 3, spectra are partitioned into three regions with regards to frequency. The first region, associated with low frequencies ($f < 0.05$ Hz for the commercial configuration, and $f < 0.03$ Hz for the prototype configuration), shows the turbulence-
220 production subrange. There, the large energy-containing eddies are responsible for the energy exchange between the mean flow and the turbulence. In this frequency subdomain, the slope of the spectra is less steep than the $f^{-5/3}$ slope. This is a manifestation of the large-scale anisotropy of the large eddies which may be advecting through the measurement site without participating directly in the energy cascade.

In the second region, at mid-frequencies, spectra associated with each beam are superimposed. This allows the identification
225 of an isotropic region of tridimensional turbulence following the $f^{-5/3}$ slope. This is the inertial subrange. The prototype configuration allows the identification of this subrange across a frequency band 9 times broader than that identified by spectra derived from measurements of the commercial configuration. For the prototype configuration, the inertial subrange is associated with eddies of time scales ranging within the frequency range 0.03 Hz $< f < 0.3$ Hz, whereas the commercial configuration allows for an identification of an inertial subrange for a frequency range 0.05 Hz $< f < 0.08$ Hz.

230 In the third region, associated with higher frequencies ($f > 0.08$ Hz for the commercial configuration, and $f > 0.3$ Hz for the prototype configuration), the spectra become flat (Fig. 3) as a manifestation of the instrument inherent Doppler noise which induces a constant spectral density, N_i , and variance, n_i^2 , for each i -th beam. Note that, N_i does not contaminate only the

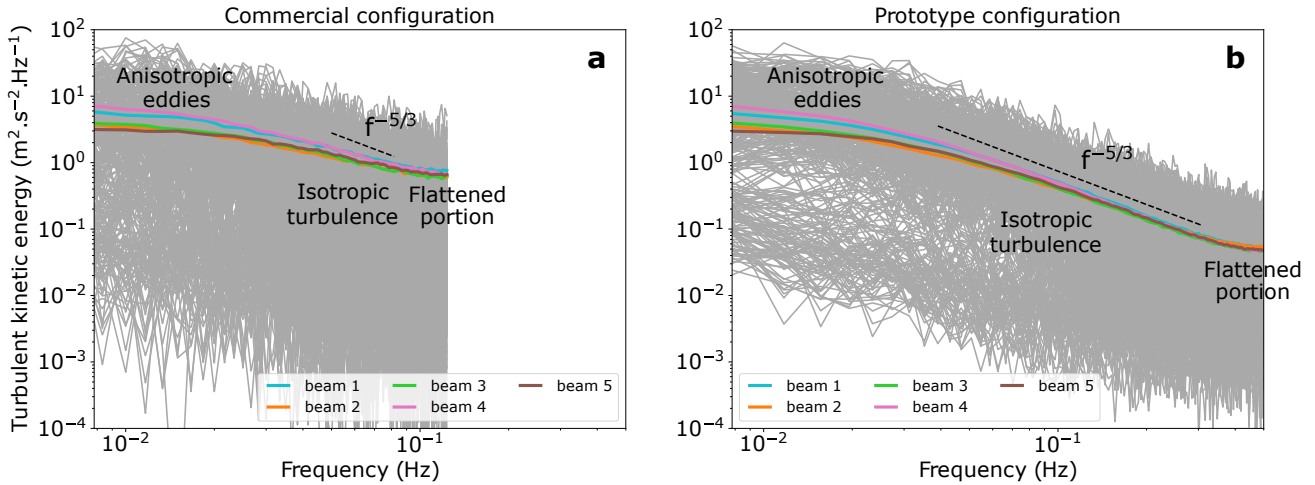


Figure 3. Individual spectra (all beams, grey fine lines) of the LOS velocities computed within 10-min temporal windows and derived from the 47-day dataset. The mean spectra associated with each beam are shown by thick lines. Black dashed lines show the classic $f^{-5/3}$ slope.

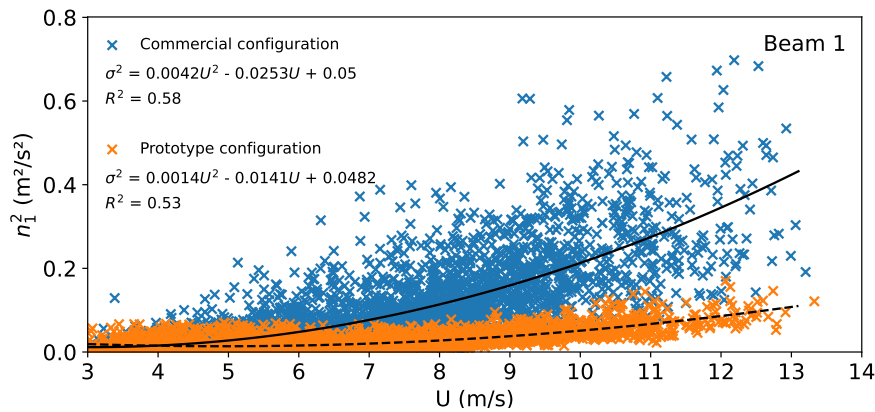


Figure 4. Doppler noise-induced variance, n_i^2 , associated with the LOS measurements of Beam 1 of the commercial (blue crosses) and prototype (orange crosses) lidars, against the mean flow speed U . Quadratic best-fit of the distributions of n_i^2 obtained from the measurements of the commercial and prototype configurations are shown by the solid and dashed black curves respectively. The equation and the coefficient of determination, R^2 , of both quadratic regressions are also shown.

higher frequency subrange but rather propagates at all frequencies, i.e., the production and inertial subranges are also impacted by the Doppler noise.



235 3.2 Doppler noise

The turbulence microscales that limit the inertial subrange are of the order of the Kolmogorov microscale, $\eta = (\nu^3/\varepsilon)^{1/4}$, where ν is the kinematic viscosity and ε , the TKE dissipation rate. Previous works dealing with the characterization of the TKE dissipation rate from wind observations showed ε estimates ranging from 10^{-6} to $10^{-3} \text{ m}^2\text{s}^{-3}$ (Chen, 1974; Siebert et al., 2003; O'Connor et al., 2010) which gives associated Kolmogorov microscale ranging from 10^{-3}m to 10^{-4}m . Considering a
240 wind field advected at a mean velocity of $\mathcal{O}(10)$ m/s, it is expected that the inertial subrange will extend to a frequency of 10^4 - 10^5 Hz. This is far beyond the Nyquist frequency, f_N , of the commercial and prototype configuration, i.e., 0.125 Hz and 0.5 Hz respectively. Thus, spectra derived from wind measurements of both configurations are expected to exhibit an inertial subrange extended up to the Nyquist frequency. However, this theoretical behavior is not observed in Fig. 3. Instead, the spectra start flattening at $f \approx 0.7f_N$, resulting from the contamination of the variance by the inherent Doppler noise. This noise is generated
245 by random scatterer motions within the sample volumes (Voulgaris and Trowbridge, 1998), i.e., the probe volumes of the lidars.

The first step in removing the Doppler noise-induced variance is the determination of the associated constant spectral density, N_i , for each i -th beam. The determination of N_i requires the identification of the characteristic frequency F . In this paper, the characteristic frequency is set to $F = 0.8f_N$. The characteristic frequency is chosen to ensure that the spectra are completely flat at frequency $f \geq F$ and thus only noise is considered when characterizing the Doppler noise. N_i is then estimated by
250 averaging the spectral densities associated with the frequency range $F \geq f \geq f_N$. Setting F at 80% of the Nyquist frequency, instead of 90%, for example, guarantee a wider frequency range to do the averaging of the spectral densities and eventually get more accurate values of N_i . The Doppler noise-induced variance, n_i^2 , is then derived from N_i and f_N following Eq. 4 and subtracted to the variance of the LOS velocities to derive noise-corrected estimates of the normal stresses and thus, proper TI estimates.

255 A potential relationship of the Doppler noise-induced variance to the mean flow speed was investigated. Fig. 4 illustrates this analysis for n_i^2 estimates associated with Beam 1 of the commercial and prototype lidars. This figure shows that the commercial configuration generates n_i^2 estimates significantly higher than that derived from the prototype configuration. The mean and standard deviation to the mean of n_i^2 estimates associated with the commercial configuration were found to be approximately 3 times higher than that associated with the prototype configuration. To supplement the analysis, the distributions of n_i^2 estimates
260 against the mean flow speed were fitted by polynomial expressions of different degrees. The best coefficient of regression, R^2 , was found when fitting the distribution with a quadratic expression. Such fitting gives R^2 values ranging from 0.43 to 0.62 depending on the beam. The highest values of R^2 were found to be associated with the prototype configuration.

3.3 Vertical stress

The variance method relies on the homogeneity of flow statistics (mean and variance) between beams. This assumption needs
265 to be validated in order to improve the level of confidence of TI estimates derived from this method. The WindCube v2.1 allows for a direct measurement of the vertical stress through the calculation of the variance of the LOS velocities measured by Beam 5, i.e., $\overline{b_5^2}$. The vertical stress can also be calculated from the mathematical expression of $\overline{w'^2}$ (Eq. 10). Estimates of $\overline{b_5^2}$ and $\overline{w'^2}$

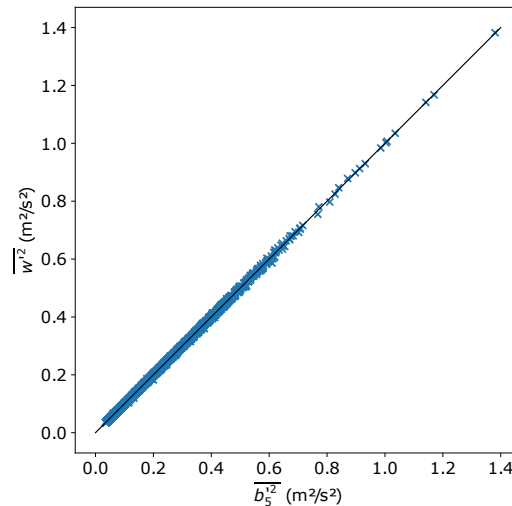


Figure 5. Vertical variance calculated with the Dewey and Stringer's formulation, $\overline{w'^2}$, versus the variance measured directly by Beam 5, $\overline{b_5'^2}$ of the prototype configuration. The black line indicates perfect agreement.

were compared considering $\overline{b_5'^2}$ as the reference. Results of this analysis associated with the prototype configuration are shown in Fig. 5. For this configuration, the mean and maximum absolute relative errors between $\overline{w'^2}$ and $\overline{b_5'^2}$ were found to be less than 1% and 5.4% respectively. For the commercial configuration, the mean and maximum absolute relative errors were found to be slightly higher, i.e., 1.2% and 5.9% respectively.

3.4 Turbulence intensity

The distributions of the TI estimates derived from the sonic anemometer measurements against that derived from measurements of both configurations were investigated during stable and unstable atmospheric conditions. Moreover, for each configuration, the efficiency of the standard and variance methods in reconstructing TI was evaluated. Fig. 6 shows the preliminary results of this analysis. From this figure one can say that, regardless the method used, there is no significant differences in TI estimates when using the commercial or prototype configuration. Besides, the behavior of the TI distributions are not governed by the wind speed as well as the atmospheric conditions. The main difference comes from the choice of the method. The standard method generates TI estimates systematically biased high. The variance method, corrected from Doppler noise, gives TI distribution aligned with the reference line, i.e., $y = x$ (equal TI derived from the sonic anemometer and the lidar). Best fit of the TI distributions derived from the variance method gives, on average, slope values 6% lower than that of the reference line, whereas slope of the best fit of the TI distributions derived from the standard method are almost 30% higher than the reference slope. Moreover, the variance method gives y -intercept from 2 to 3 times lower than that derived from the standard method.

However, the use of the variance method generates scattered distributions. This results in lower coefficient of determination, R^2 , of the best fit of the TI distributions in comparison to R^2 given by the standard method. The scattered distributions are

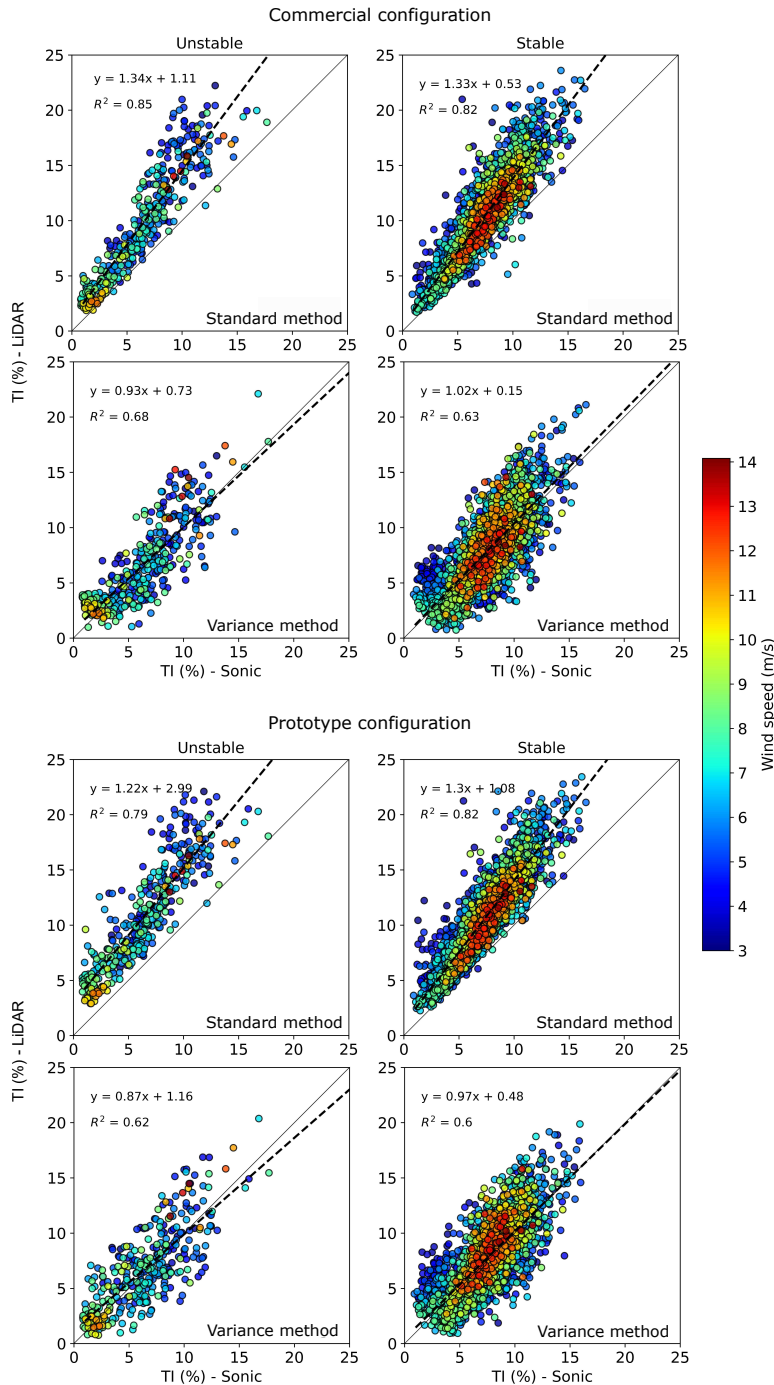


Figure 6. Distributions of TI estimates derived from the sonic anemometer measurements against that derived from the standard and variance applied on measurements of the commercial and prototype configurations under stable and unstable atmospheric conditions. Solid black lines show the line of perfect agreement between TI estimates derived from the sonic anemometer and the lidar. Dashed black lines are the best fit of the distributions. Color scale accounts for the mean flow speed.



Configurations	Commercial				Prototype			
	Stable		Unstable		Stable		Unstable	
Methods	Standard	Variance	Standard	Variance	Standard	Variance	Standard	Variance
Q_1 (%)	36.7	10.0	44.3	13.2	35.0	9.1	50.9	13.0
Q_2 (%)	50.5	21.4	62.2	26.2	49.6	19.8	73.0	28.2
Q_3 (%)	66.8	37.6	92.3	51.5	62.2	33.7	113.0	52.3

Table 1. First, second and third quartiles of the absolute relative error between TI estimates derived from the sonic anemometer measurements (reference) against that derived from the standard (given TI_s) and variance (given TI_v) applied on measurements of the commercial and prototype configurations under stable and unstable atmospheric conditions.

the result of the Doppler noise-induced variance correction of TI estimates. The noise correction is not made on individual fluctuations but rather on the mean fluctuation averaged over each 10-min ensemble. Thus, the noise correction is sensitive to the number of realizations considered and Doppler noise will always result in some spreading of the corrected TI estimates.

The error in the reconstruction of TI by the standard and variance methods applied on measurements derived from the commercial and prototype configurations was quantified with the calculation of the absolute relative error, ξ , considering sonic-derived TI as reference. The first, second (median) and third quartiles of the absolute relative error were investigated for TI calculated from measurements collected during stable and unstable conditions. Results are compiled in Table 1 and illustrated in Fig. 7. Each quartile gives absolute relative error higher under unstable conditions than under stable conditions, regardless of the configurations and methods used. Under stable conditions and for the standard and variance methods, ξ associated with the prototype configuration is slightly lower than ξ associated with the commercial configuration. The median of the TI absolute relative error associated with the standard method is approximately 50% for both configurations. With the use of the variance method, the median of the TI absolute relative error drops to 20%. Under unstable conditions, ξ associated with the commercial configuration is slightly lower. Moreover, for both configurations, the use of the variance method applied on measurements collected under unstable conditions reduced the error ξ by a factor of 2.5 in comparison to the standard method.

The variance method involves the formulation of $\overline{u'^2}$ and $\overline{v'^2}$ proposed by Dewey and Stringer (2007) and the explicit removal of the Doppler noise-induced variance to the variance of the LOS velocities measured by each beam. The relevance of the noise-removal in providing proper TI estimates has been studied (Fig. 8). For each configuration, cumulative distribution functions (CDF) of TI estimates derived from the variance method including a removal of Doppler noise are shown alongside CDF of TI estimates derived from the variance method, applied without consideration of the Doppler noise. For comparison, CDF of TI derived from measurements of the sonic anemometer and the standard method are also illustrated. The CDF were calculated considering the 4336 10-min subsets, i.e., no distinction was made regarding the atmospheric stability.

The CDFs range from 0 to 1 with step equal to $1/4336$. At each step, the relative error between the associated reference TI, given by the sonic anemometer, and TI given by the standard or variance (with and without noise removal) method applied on measurements provided by the commercial or prototype configuration was calculated. The mean relative error was then

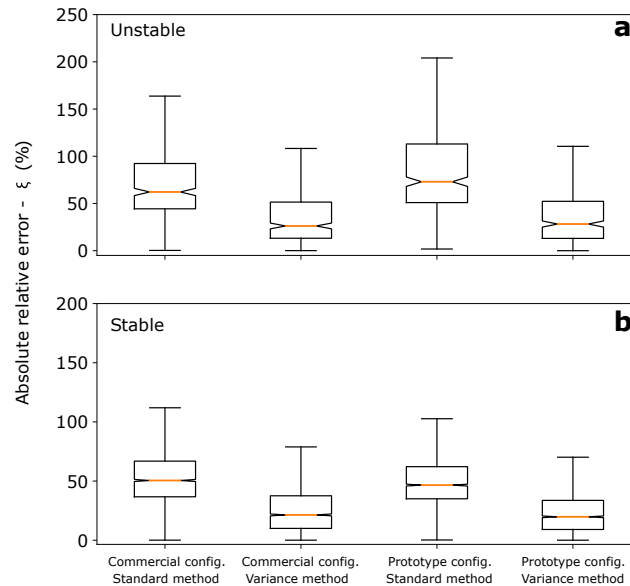


Figure 7. Boxplots of the absolute relative error, ξ , in TI estimates derived from the standard (given TI_s) and variance (given TI_v) applied on measurements of the commercial and prototype configurations under stable and unstable atmospheric conditions.

computed. Table 2 shows that the lowest mean relative errors are associated with the prototype configuration. The gap between the mean error associated with the commercial configuration and that associated with the prototype configuration is minimum, i.e. 2.1%, for TI estimated from the standard method. This gap is 10 times higher for TI estimated from the variance method including the removal of the Doppler noise. For both configurations, results show that the standard method generates an overestimation of TI by more than 50%. The use of the variance method, without consideration of Doppler noise, reduces this gap to approximately 30%. A significant improvement is found when using the variance method combined with the removal of the Doppler noise. This reduces the error in TI estimation by a factor of 3.2 for TI derived from measurements of the commercial configuration and by a factor of 3.9 for TI derived from measurements of the prototype configuration, in comparison to TI derived from the standard method (Table 2). Moreover, the use of the prototype configuration enables an improvement of TI estimates by 4.5% when using the standard method and 2.7% when using the variance method, in comparison to TI estimates associated with the commercial configuration.

4 Discussion

This paper presents a new method to derive TI from measurements of a WindCube v2.1 lidar. This method requires the assumption that the fluctuations in the flow are statistically homogeneous, i.e., at a given altitude, the beams sample turbulence fields that have the same statistics. Therefore, the assumption of spatial homogeneity between the beams is made only in the mean and variance of the LOS velocity signal and not on the instantaneous LOS velocities which are inhomogeneous between

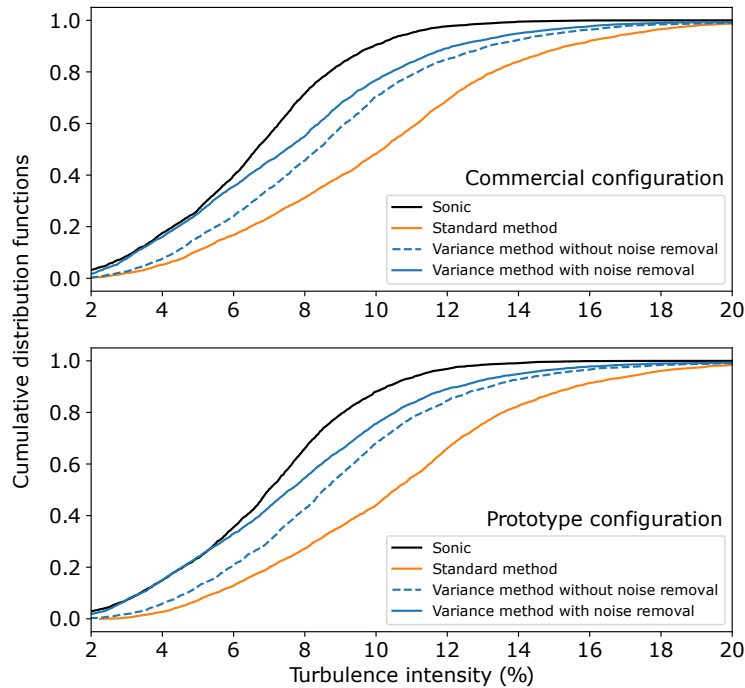


Figure 8. Cumulative distribution functions (CDF) of TI estimates derived from the standard and variance methods applied on measurements of the commercial and prototype configurations. A distinction is made on CDF derived from the variance method including an explicit removal of the Doppler noise (solid blue curve), as it is done throughout this paper, and CDF derived from the variance method without consideration of Doppler noise (dashed blue curve). The reference CDF associated with measurements of the sonic anemometer is represented by the black curves.

Configurations	Commercial	Prototype
Standard method	53.4%	52.3%
Variance method without noise removal	30.8%	28.1%
Variance method with noise removal	16.7%	13.2%

Table 2. Mean error in TI estimation derived from the standard and variance (with and without Doppler noise removal) methods applied on measurements collected by the commercial and prototype configurations. The errors are calculated considering TI derived from measurements of the sonic anemometer as reference.

the beams. The assumption of spatial homogeneity has been tested by comparing the variance of the vertical velocity, given directly by Beam 5, and the variance of the vertical velocity resolved by the Dewey and Stringer’s formulation. The results show that the gap between the measured and resolved vertical velocity variance is slightly higher than 1% for both configurations.

330 This result supports the validity of the spatial homogeneity of the statistics of the turbulence fields. Moreover, the low gap



between the measured and resolved vertical velocity variance supports the relevance of the variance method to calculate the Reynolds stresses and thus, TI.

However, one should be aware that the technical characteristics of the WindCube v2.1, or any other pulsed lidar, limit the level of turbulent energy that is detectable by this technology. A first limitation of the profiling pulsed lidars in resolving turbulence is the vertical resolution, i.e., probe length of the lidar. The lidar performs some spatial averaging within its probes, thus limiting the range of eddies for which it will retain information. With probe lengths of 20 m, eddies of size smaller than twice (to avoid aliasing) the length of the probe lengths will not be resolved by the WindCube v2.1 and the variance in the velocity field will be reduced. As a result, turbulence metrics will be systematically biased low. Another lidar limitation is the use of diverging beams. This means that the area, i.e. the beam spread Δb , in which the measurements are being integrated increases with increasing altitude, changing the spatial averaging of the turbulence metrics. The beam spread is a function of height, H , above ground such that $\Delta b = 2H \tan \theta$. At a given altitude, the beam spread is the limited length scale (and associated time scale) that can be measured accurately by a lidar. The present study focused on the 97-m altitude. Considering the beams inclination, $\theta = 28^\circ$ of the WindCube v2.1, the beam spread between two opposite beams is approximately 103 m which matches the land-based wind turbines rotor diameter. Considering the Taylor's assumption of frozen turbulence, an appropriate sampling rate, \hat{f} , to capture the eddies of size similar to Δb is given by $\hat{f} = U/\Delta b$. Thus, at 97-m altitude the commercial configuration which samples at $f_c = 0.25$ Hz will capture the eddies of size higher than the beam spread as long as the flow is advected by a mean velocity of approximately 26 m/s. This is slightly higher than the cut-out speed of the operational wind turbines deployed worldwide. For the prototype configuration, which samples 4 times faster than the commercial configuration, this velocity threshold is more than 100 m/s. This is beyond the velocity range of interest for the wind industry.

More likely, wind turbines will respond to turbulence on scales similar to the rotor diameters [$\mathcal{O}(100)$ m] and also the blade chord lengths [$\mathcal{O}(1)$ m]. The commercial configuration is sufficient to capture the largest turbulence length scales [$\mathcal{O}(100)$ m] of interest for the purpose of turbine design specifications. However, the sampling rate of the commercial configuration is not sufficient to capture turbulence eddies of size matching the dimension of the blade chord lengths. At 97-m altitude, turbulence eddies of size comprises within 1 to 5 m and advected at a mean flow speed of 10 m/s would require a sampling rate of 10 Hz to capture the smallest eddies and 2 Hz to capture the largest eddies. This is respectively 40 and 8 times faster than the sampling rate of the commercial configuration. Note that, in practice, the appropriate sampling rates mentioned so far should be twice higher in order to avoid aliasing effects during signal processing.

An increase of the sampling rate has been investigated in this paper using a prototype configuration of the WindCube v2.1. This configuration samples 4 times faster than the commercial configuration. The variance method applied on measurements collected by the prototype configuration enables an improvement of TI estimates by approximately 3% in comparison to turbulence estimates given by the commercial configuration. These gaps are due to the capability of the prototype configuration in capturing turbulent energy associated with smaller eddies, not detectable by the commercial configuration. Moreover, the prototype configuration captured inertial subranges of the LOS velocity spectra across a frequency domain 9 times wider than the spectra derived from measurements of the commercial configuration. These results offer valuable perspectives for the examination of the TKE budget which involves the TKE dissipation rate calculating directly from the LOS velocity spectra



given by Beam 5 and the TKE production rate which can be fully resolved from the Dewey and Stringer's formulations. Evaluating the TKE budget will reinforce the understanding of the dynamics of the turbulence and, eventually, improve the ability of numerical models to reconstruct the wind flow dynamics.

Investigating the small turbulence scales from measurements of pulsed lidars depends on the ability in removing the inherent
370 Doppler noise. The Doppler noise results from errors in measuring the frequency change or phase shift of the reflected pulses. Results presented in this paper show that the Doppler noise depends on the sampling rate. The prototype configuration reduces the noise level by a factor of 3 in comparison to the commercial configuration. A faster sampling rate will thus reduce the Doppler noise as it will be redistributed along a wider frequency range. The Doppler noise also depends on the pulses length, i.e., probes length of the lidars. Lower probes length will enable to capture smaller eddies but with an increased Doppler noise.
375 The size of the probe lengths is thus a tradeoff between longer pulses (i.e., longer probe length) with lower Doppler noise and shorter pulses (i.e., smaller probe length) with higher Doppler noise and thus higher raw TI. Although the removal of the Doppler noise-induced variance demonstrated significant improvement of TI estimation, the theoretical correction for Doppler noise is imperfect. Thus, it is preferable to use large probe length in order to reduce the amount of noise that must be later removed from raw TI. Ideally, the probe length would be set so as to require Doppler noise values that are notably smaller than
380 the expected turbulent fluctuations.

For many years it has been a matter of great interest in the wind energy community as to whether atmospheric stability influences turbulence and thus wind turbine loads or wake (Magnusson and Smedman, 1994; Sathe et al., 2013; Abkar and Porté-Agel, 2015). Atmospheric stability has been demonstrated to influence mainly the rotor loads whereas the blade loads are hardly influenced (Sathe et al., 2013). In the present paper, the ability of both configurations in measuring turbulence has been
385 studied under stable and unstable atmospheric conditions. The standard and variance method were found to be less efficient during unstable conditions with higher errors in TI estimation. During unstable conditions, the length scales of turbulence are known to increase whereas, during stable conditions, they decrease (Peña et al., 2010; Sathe and Mann, 2013). Thus, during unstable conditions the lidar measures much larger values of variance due to the larger turbulent motions present under these conditions. The higher error in TI estimates can be attributed to the cross-contamination effect which artificially increases the
390 level of variance measured by lidars and is more prominent under unstable conditions (Sathe et al., 2011). This result suggests that despite the considerable improvement of TI estimation, the variance method combined with an explicit removal of Doppler noise does not eliminate but rather attenuates substantially the cross-contamination effect. The most effective way to annihilate the cross-contamination effect would be to record simultaneously the LOS velocities associated with each beam of the lidar instead of swinging from one beam to another.

395 5 Conclusion

The variance method presented in this paper demonstrates a considerable improvement for TI estimation derived from wind measurements collected by pulsed lidars employing the Doppler beam swinging technique. The variance method applied on measurements collecting by the commercial configuration of the WindCube v2.1 allows for a reduction in TI estimation by a



factor of 3.2 in comparison to estimates given by the standard method, and by a factor of 3.9 for TI derived from measurements
400 of the prototype configuration. This highlights the need for developing lidars operating at faster sampling rates. Currently,
the sampling rate of the commercial configuration allows for capturing the turbulence length scales of size similar to the rotor
diameter of wind turbines. Capturing smaller turbulence length scales, for example matching the size of the blade chord lengths,
will require faster sampling rates. The prototype configuration has been developed specifically for this purpose and constitutes
a valuable first step toward the development of the new generation of pulsed lidars. However, efforts still need to be made to
405 increase the sampling rate to at least twice higher than that of the prototype configuration. This will allow for capturing the
smallest turbulence length scales of interest for the purpose of turbine design specifications.

The variance method is based on the LOS velocities. It is thus critical that developers of the next generation of lidars
made systematically available the LOS velocities as output measurements of their device. Ideally, the recording of the LOS
velocities provides by each beam should be done simultaneously to annihilate the cross-contamination effect and thus provide
410 TI estimates even more accurate. The developers of the new generation of pulsed lidars should also investigate the possibility
to reduce the beam inclination, θ , in order to reduce the beam spread and thus the limit of the turbulence length scales that can
be measured accurately by a lidar. Moreover, the variance method includes an explicit removal of the Doppler noise-induced
variance. Failing to account for Doppler noise when characterizing turbulence would result in unnecessarily high factors of
safety and associated costs. A proper use of the variance method by developers and operators of future wind farms as well as
415 wind turbine manufacturers will substantially improve the site assessment stage. It is expected that this method will contribute
to improve the survivability, reliability and performance of wind farms, eventually enabling more profitable wind projects and
lower investment costs due to optimized designs.

One should know that the variance method presented in this paper has been validated for ground-based lidars and thus can
be applied only for onshore wind energy applications. The deployment of this method for offshore wind energy applications is
420 the next step. The site assessment stage of offshore wind projects usually include measurements of lidar units integrated onto a
standalone floating structure, such as buoys which exhibit translational (surge, sway and heave) and rotational motions (pitch,
roll and yaw). All of these motions have the potential to adversely affect wind measurements collected by a lidar. In particular,
on a buoy, pitch and roll alter the LOS velocities and add additional variance in the signal that need to be filter to provide
proper TI estimates. Thus, for offshore applications, the variance method needs to be customized by including a correction of
425 the buoy-induced variance in TI estimation.

Author contributions. Maxime Thiébaud: Conceptualization; Methodology; Analysis; Investigation; Writing original draft. Marie Cathelain:
Writing original draft. Salma Yahiaou: Development of the prototype WindCube v2.1. Ahmed Esmail: Data acquisition.

Competing interests. The authors declare that they have no conflict of interest.



Data availability. Raw data of the prototype lidar and the sonic anemometer will be made publicly available

430 *Acknowledgements.* This work was supported by France Energies Marines and the French government, managed by the Agence Nationale de la Recherche under the Investissements d'Avenir program, with the reference ANR-10-IEED-0006-34. This work was carried out in the framework of the POWSEIDOM projects.



References

- Abkar, M. and Porté-Agel, F.: Influence of atmospheric stability on wind-turbine wakes: A large-eddy simulation study, *Physics of fluids*, 435 27, 035 104, publisher: AIP Publishing LLC, 2015.
- Browning, K. A. and Wexler, R.: The determination of kinematic properties of a wind field using Doppler radar, *Journal of Applied meteorology and climatology*, 7, 105–113, 1968.
- Canadillas, B., Bégué, A., and Neumann, T.: Comparison of turbulence spectra derived from LiDAR and sonic measurements at the offshore platform FINO1, in: *Proceedings of the 10th German Wind Energy Conference, DEWEK*, 2010.
- 440 Chen, W. Y.: Energy dissipation rates of free atmospheric turbulence, *Journal of Atmospheric Sciences*, 31, 2222–2225, 1974.
- Clifton, A. and Wagner, R.: Accounting for the effect of turbulence on wind turbine power curves, in: *Journal of Physics: Conference Series*, vol. 524, p. 012109, IOP Publishing, issue: 1, 2014.
- Dewey, R. and Stringer, S.: Reynolds stresses and turbulent kinetic energy estimates from various ADCP beam configurations: Theory, *J. of Phys. Ocean*, pp. 1–35, 2007.
- 445 Durgesh, V., Thomson, J., Richmond, M. C., and Polagey, B. L.: Noise correction of turbulent spectra obtained from acoustic doppler velocimeters, *Flow Measurement and Instrumentation*, 37, 29–41, 2014.
- Emeis, S., Harris, M., and Banta, R. M.: Boundary-layer anemometry by optical remote sensing for wind energy applications, *Meteorologische Zeitschrift*, 16, 337–348, publisher: Berlin: Borntraeger, c1992-, 2007.
- Frish, U.: *The legacy of A.N. Kolmogorov*, Cambridge University Press, 1995.
- 450 Gottschall, J., Courtney, M. S., Wagner, R., Jørgensen, H. E., and Antoniou, I.: Lidar profilers in the context of wind energy—a verification procedure for traceable measurements, *Wind Energy*, 15, 147–159, publisher: Wiley Online Library, 2012.
- Guerra, M. and Thomson, J.: Turbulence Measurements from Five-Beam Acoustic Doppler Current Profilers, *Journal of Atmospheric and Oceanic Technology*, 34, 1267–1284, 2017.
- Howland, M. F., Lele, S. K., and Dabiri, J. O.: Wind farm power optimization through wake steering, *Proceedings of the National Academy of Sciences*, 116, 14 495–14 500, publisher: National Acad Sciences, 2019.
- 455 Jonkman, J. and Kilcher, L.: *TurbSim User’s Guide: Version 1.06.00*, National Renewable Energy Laboratory, Tech. rep., 2012.
- Kelberlau, F. and Mann, J.: Cross-contamination effect on turbulence spectra from Doppler beam swinging wind lidar, *Wind Energy Science*, 5, 519–541, publisher: Copernicus GmbH, 2020.
- Kelley, N. D., Jonkman, J., Scott, N., Bialasiewicz, J., and Redmond, L.: The Impact of Coherent Turbulence on Wind Turbine Aeroelastic Response and Its Simulation, *WindPower 2005 Conference, NREL/CP-500-38074*, August, 2005.
- 460 Kelley, N. D., Jonkman, B. J., and Scott, G. N.: *Great Plains Turbulence Environment: Its Origins, Impact, and Simulation*, Tech. rep., National Renewable Energy Lab.(NREL), Golden, CO (United States), 2006.
- Kim, D., Kim, T., Oh, G., Huh, J., and Ko, K.: A comparison of ground-based LiDAR and met mast wind measurements for wind resource assessment over various terrain conditions, *Journal of Wind Engineering and Industrial Aerodynamics*, 158, 109–121, publisher: Elsevier, 465 2016.
- Magnusson, M. and Smedman, A.-S.: Influence of atmospheric stability on wind turbine wakes, *Wind Engineering*, pp. 139–152, publisher: JSTOR, 1994.
- McMillan, J. M. and Hay, A. E.: Spectral and structure function estimates of turbulence dissipation rates in a high-flow tidal channel using broadband ADCPs, *Journal of Atmospheric and Oceanic Technology*, 34, 5–20, 2017.



- 470 Newman, J. F., Klein, P. M., Wharton, S., Sathe, A., Bonin, T. A., Chilson, P. B., and Muschinski, A.: Evaluation of three lidar scanning strategies for turbulence measurements, *Atmospheric Measurement Techniques*, 9, 1993–2013, publisher: Copernicus GmbH, 2016.
- O'Connor, E. J., Illingworth, A. J., Brooks, I. M., Westbrook, C. D., Hogan, R. J., Davies, F., and Brooks, B. J.: A method for estimating the turbulent kinetic energy dissipation rate from a vertically pointing Doppler lidar, and independent evaluation from balloon-borne in situ measurements, *Journal of atmospheric and oceanic technology*, 27, 1652–1664, 2010.
- 475 Peña, A., Gryning, S.-E., and Mann, J.: On the length-scale of the wind profile, *Quarterly Journal of the Royal Meteorological Society*, 136, 2119–2131, publisher: Wiley Online Library, 2010.
- Pope, S. B.: *Turbulent flows*, Cambridge University Press, 2000.
- Richard, J.-B., Thomson, J., Polagye, B., and Bard, J.: Method for identification of doppler noise levels in turbulent flow measurements dedicated to tidal energy, *International Journal of Marine Energy*, 3, 52–64, 2013.
- 480 Rohrig, K., Berkhout, V., Callies, D., Durstewitz, M., Faulstich, S., Hahn, B., Jung, M., Pauscher, L., Seibel, A., and Shan, M.: Powering the 21st century by wind energy—Options, facts, figures, *Applied Physics Reviews*, 6, 031 303, publisher: AIP Publishing LLC, 2019.
- Sathe, A. and Mann, J.: Measurement of turbulence spectra using scanning pulsed wind lidars, *Journal of Geophysical Research: Atmospheres*, 117, publisher: Wiley Online Library, 2012.
- Sathe, A. and Mann, J.: A review of turbulence measurements using ground-based wind lidars, *Atmospheric Measurement Techniques*, 6, 3147–3167, publisher: Copernicus GmbH, 2013.
- 485 Sathe, A., Mann, J., Gottschall, J., and Courtney, M. S.: Can wind lidars measure turbulence?, *Journal of Atmospheric and Oceanic Technology*, 28, 853–868, 2011.
- Sathe, A., Mann, J., Barlas, T., Bierbooms, W., and Van Bussel, G. J. W.: Influence of atmospheric stability on wind turbine loads, *Wind Energy*, 16, 1013–1032, publisher: Wiley Online Library, 2013.
- 490 Sathe, A., Mann, J., Vasiljevic, N., and Lea, G.: A six-beam method to measure turbulence statistics using ground-based wind lidars, *Atmospheric Measurement Techniques*, 8, 729–740, publisher: Copernicus GmbH, 2015.
- Siebert, H., Wendisch, M., Conrath, T., Teichmann, U., and Heintzenberg, J.: A new tethered balloon-borne payload for fine-scale observations in the cloudy boundary layer, *Boundary-layer meteorology*, 106, 461–482, publisher: Springer, 2003.
- Sjöholm, M., Mikkelsen, T., Mann, J., Enevoldsen, K., and Courtney, M.: Time series analysis of continuous-wave coherent Doppler lidar wind measurements, in: *IOP Conference Series: Earth and Environmental Science*, vol. 1, p. 012051, IOP Publishing, issue: 1, 2008.
- 495 Smith, D. A., Harris, M., Coffey, A. S., Mikkelsen, T., Jørgensen, H. E., Mann, J., and Danielian, R.: Wind lidar evaluation at the Danish wind test site in Høvsøre, *Wind Energy: An International Journal for Progress and Applications in Wind Power Conversion Technology*, 9, 87–93, publisher: Wiley Online Library, 2006.
- Strauch, R. G., Merritt, D. A., Moran, K. P., Earnshaw, K. B., and De Kamp, D. V.: The Colorado wind-profiling network, *Journal of Atmospheric and Oceanic Technology*, 1, 37–49, 1984.
- 500 Thiébaud, M., Filipot, J.-F., Maisondieu, C., Damblans, G., Duarte, R., Droniou, E., Chaplain, N., and Guillou, S.: A comprehensive assessment of turbulence at a tidal-stream energy site influenced by wind-generated ocean waves, *Energy*, 191, 116 550, 2020a.
- Thiébaud, M., Filipot, J.-F., Maisondieu, C., Damblans, G., Jochum, C., Kilcher, L. F., and Guillou, S.: Characterization of the vertical evolution of the three-dimensional turbulence for fatigue design of tidal turbines, *Philosophical Transactions of the Royal Society A*, 378, 20190 495, publisher: The Royal Society Publishing, 2020b.
- 505 Thomson, J., Polagye, B., Richmond, M., and Durgesh, V.: Quantifying turbulence for tidal power applications, in: *OCEANS 2010*, pp. 1–8, IEEE, 2010.



- Thomson, J., Polagye, B., Durgesh, V., and Richmond, M. C.: Measurements of turbulence at two tidal energy sites in Puget Sound, WA, *Oceanic Engineering, IEEE Journal of Oceanic Engineering*, 37, 363–374, 2012.
- 510 Veers, P., Dykes, K., Lantz, E., Barth, S., Bottasso, C. L., Carlson, O., Clifton, A., Green, J., Green, P., and Holttinen, H.: Grand challenges in the science of wind energy, *Science*, 366, eaau2027, publisher: American Association for the Advancement of Science, 2019.
- Voulgaris, G. and Trowbridge, J. H.: Evaluation of the acoustic Doppler velocimeter (ADV) for turbulence measurements, *Journal of atmospheric and oceanic technology*, 15, 272–289, publisher: American Meteorological Society, 1998.
- Wagner, R., Courtney, M., Gottschall, J., and Lindelöw-Marsden, P.: Accounting for the speed shear in wind turbine power performance
515 measurement, *Wind Energy*, 14, 993–1004, publisher: Wiley Online Library, 2011.
- Wharton, S. and Lundquist, J. K.: Atmospheric stability affects wind turbine power collection, *Environmental Research Letters*, 7, 014 005, publisher: IOP Publishing, 2012.